Géotechnique **00**, 1–16 [http://dx.doi.org/10.1680/geot.XX.XXXXX]

Backward Erosion Piping in Geotechnical Infrastructure: A Rate Process Perspective

ZHIJIE WANG*, CAGLAR OSKAY†, ALESSANDRO FASCETTI*

Backward erosion piping (BEP) has been recognized as a major cause of failures in water-retaining structures. However, the fundamental mechanisms controlling the phenomenon are not well understood. This research applies the theory of rate processes to develop a constitutive relationship between energy density of the seepage flow and the erosion rate of soils during the evolution of BEP. The resulting equation is used to analyze four datasets of previously reported experimental observations. The mechanical parameters estimated through the proposed model fall into the ranges of values that were reported in the literature. To validate the proposed approach, the constitutive model was incorporated into a multiphase numerical framework to simulate evolution of BEP in embankment soil and compared with reported experimental observations. The numerical framework with the proposed constitutive model is shown to be capable of reproducing both the observed evolution of local hydraulic gradients and pipe progression in the structure.

KEYWORDS: backward erosion piping; rate process; flow energy; constitutive modeling

INTRODUCTION

Internal erosion is considered to play a leading role in embankment dam failures, as it has been attributed as cause of approximately one half of embankment failures worldwide (Foster et al., 2000). According to the International Commission on Large Dams (ICOLD), there are four types of internal erosion based on their failure mechanisms: suffusion, concentrated leaks, contact erosion, and backward erosion (ICOLD, 2013). The properties of the soils in an embankment or in its foundation determine its vulnerability to which of these erosion mechanisms. Suffusion occurs in widely graded or gap-graded cohesionless soils where finer particles are eroded through pores between coarser particles by seepage flow. Concentrated leaks occur in plastic soils, or unsaturated silts and sands, where an opening exits and is enlarged as soil particles are eroded by the leaking water. Contact erosion occurs on the contact interface of a coarser soil, such as a gravel, and a fine soil where flow parallel to the contact in the coarse soil erodes the fine soil. Backward erosion piping (BEP) mainly occurs in embankment foundations of cohesionless soils where soil particles under a roof of cohesive top layer are eroded by the seepage flow, and a pipe initiates at a free unfiltered surface downstream and progresses upstream causing instability of the flood protection system (Robbins, 2016; Vandenboer et al., 2018; Pol et al., 2022). BEP is the most common mechanism accounting up to one third of all internal erosion failures of embankment dams and their foundations (Richardds & Reddy, 2007). This study focuses on the development of a novel theoretical framework to describe the evolution of backward erosion piping in geotechnical infrastructure.

Due to the catastrophic consequences of BEP, a considerable amount of research has been focused on assessing the likelihood of BEP in geotechnical flood protection infrastructure (GFPI) systems. Several semi-empirical models have been proposed in the literature to evaluate the potential of BEP based on experimental observations. In these models, a central challenge has been characterizing response of soils under different hydraulic loading conditions, with an emphasis on identifying the critical hydraulic loading that initiates and propagates BEP. Hydraulic gradient and hydraulic shear stress have been proposed as measures to characterize hydraulic loading and constitutive laws have been developed to predict soil erosion rate revolving around these two quantities. Identification of the critical hydraulic gradient or the critical shear stress for pipe initiation have therefore been widely studied (Bligh, 1910; Sellmeyer, 1988; van Beek et al., 2010; Fleshman & Rice, 2013; Negrinelli, 2015; van Beek et al., 2015; Peng & Rice, 2020; Ojha et al., 2003; Reddi et al., 2000). Recently, the flow energy has been proposed as an objective measure to characterize the hydraulic loading intensity. Corresponding constitutive relationships were developed between erosion rate and flow energy based on experimental observations (Kodieh et al., 2021; Marot et al., 2012; Sibille et al., 2015).

Experimental works available in literature shed light on the characteristics of BEP and its evolution both at the laboratory (Fleshman & Rice, 2014; Richardds & Reddy, 2012; Robbins et al., 2018) and field scale (Marchi et al., 2021; Robbins et al., 2020; van Beek et al., 2011). Current strategies

Manuscript received...
*Department of Civil and Environmental Engineering, University of Pittsburgh, Pittsburgh PA, 15261
†Department of Civil and Environmental Engineering, Vanderbilt University, Nashville TN, 37235

employ semi-analytical methods or simplified schematization of the field conditions to estimate the potential for piping evolution and to guide the design of new systems as well as the retrofitting of existing ones (Brandon et al., 2018; Schmertmann, 2000; Sellmeijer et al., 2011). However, the complexity in describing the full breath of field conditions and GFPI structural arrangements (i.e., variations in geometrical features, spatial variability in soil conditions, possible presence of filters, upward sloping and pressure relief systems) makes it prohibitive to fully characterize the BEP potential experimentally. Therefore, mathematical and numerical models are required to estimate the likelihood of failure of the GFPI and inform design strategies.

Numerical approaches, which have been employed in previous studies on BEP, generally fall into three categories: (1) single-phase transport models in which the permeability of the soil is increased to simulate the progression of erosion (Fascetti & Oskay, 2019a; Robbins. & Griffiths, 2021; Vandenboer et al., 2014), (2) discrete element approaches, generally coupled with continuum descriptions for the fluid flow, to investigate localized phenomena (El Shamy & Aydin, 2008; Wang & Ni, 2013), and (3) multiphase models in which the density evolution of mobilized particles is described using regularized constitutive relationships and coupled with the groundwater flow via kinematic constraints (Fascetti & Oskay, 2019b; Papamichos & Vardoulakis, 2005; Zhang et al., 2013). The above mentioned numerical approaches utilize semi-empirical constitutive relationships based on a critical hydraulic gradient or a critical hydraulic shear stress. Moreover, the definition of a critical value of the hydraulic gradient (or tangential shear) is prohibitive in 3-dimensional problems, as the values of such parameters are highly influenced by flow direction and characteristics.

The theory of rate processes is based on statistical mechanisms and has been successfully employed to describe particulate systems undergoing time-dependent flow or deformation (Eyring, 1936; Glasstone et al., 1941). Applications of the theory of rate processes to soil behavior began in the 1960s (Andersland & Douglas, 1970; Christensen & Das, 1973; Gularte et al., 1980; Mitchell, 1964; Mitchell et al., 1968, 1969; Raudkivi & Hutchison, 1974; Murayama et al., 1984). Among the aforementioned articles, Christensen & Das (1973), Raudkivi & Hutchison (1974) and Gularte et al. (1980) dealt with surface erosion of cohesive soils, while the rest of these studies were focused on either strength or creep of soils. The reported dependencies of erosion rates on temperature and hydraulic shear stress were in agreement with the theory of rate processes (Christensen & Das, 1973; Gularte et al., 1980; Raudkivi & Hutchison, 1974). However, such theoretical framework has not yet been applied to the internal erosion process in sand which controls the evolution of BEP.

Therefore, this study aims to propose and evaluate a theoretical model, based on the theory of rate processes, to describe BEP progression in GFPI systems. The model was derived from fundamental inter-granular interactions in cohesionless soils rather than being generalized from phenomenological observations. The central component of the proposed model is a constitutive relationship between erosion rate of soil mass in time and energy density of seepage flow. The constitutive relationship is first exercised to perform non-linear regressions on four experimental internal erosion datasets reported in the literature. The mechanical parameters estimated from the regressions are in good agreement with those reported in previous studies. To illustrate its capability in describing BEP progression in GFPI, the proposed model was incorporated into a multiphase numerical framework, and simulation results were compared to reported experimental outcomes. The numerical results demonstrate that the model is capable of representing both the global BEP progression rates and local hydraulic conditions around the pipe tip. Moreover, the estimated mechanical parameters are consistent with each other and align with previously reported values for different mechanisms. To the best of the authors' knowledge, this work represents the first attempt to utilize the theory of rate processes to describe backward erosion piping.

BEP AS A RATE PROCESS

Based on review of experiments available in literature at the small-, medium-, and large-scale, BEP in geotechnical systems exhibits the following traits: 1) stochasticity, 2) complex dynamic equilibrium conditions that yield "step-wise" behavior (see Figure 2), and 3) some degree of exponential acceleration of the phenomenon when the intact portion of the system (i.e., the upstream side not yet subjected to erosion) is reduced to approximately $1/3$ of the seepage length (van Beek, 2015). These traits lead us to cast a parallelism with the theory of rate processes, in which an explicit consideration of a free energy barrier is derived that guides the evolution of the process in exam. Glasstone et al. (1941) pointed out that the theory of rate processes is not only a theory of kinetics of chemical reactions, but also one that can be applied to any process involving a rearrangement of matter, i.e., a "rate process". In fact, the theory of rate processes has been successfully used in describing different physical mechanisms in soils, such as creep, shear deformation, and surface erosion of clays (Gularte et al., 1980; Mitchell, 1964; Mitchell et al., 1968). In this study, the application of the theory of rate processes to BEP in cohesionless soils is investigated to provide insights into the fundamental nature of BEP and development of new analytical and numerical frameworks. Detailed development of the theory of rate processes may be found in Eyring (1936), Glasstone et al. (1941), and other works in the physical chemistry literature.

The theory of rate processes idealizes atoms, molecules, and/or particles participating in a flow (or deformation) process, termed as flow units, as constrained from movement relative to each other by energy barriers which separate adjacent equilibrium positions. The displacement of one mole of flow

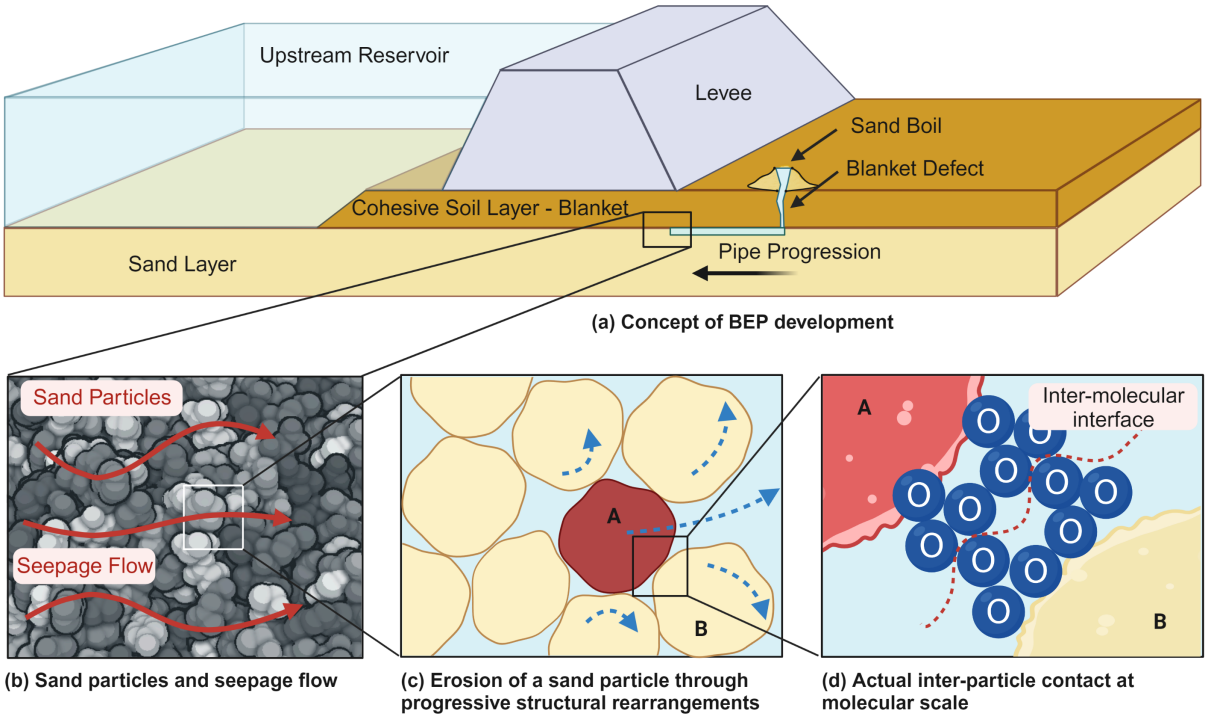

Fig. 1. A schematic of mechanisms of BEP at multiple scales (created with BioRender.com)

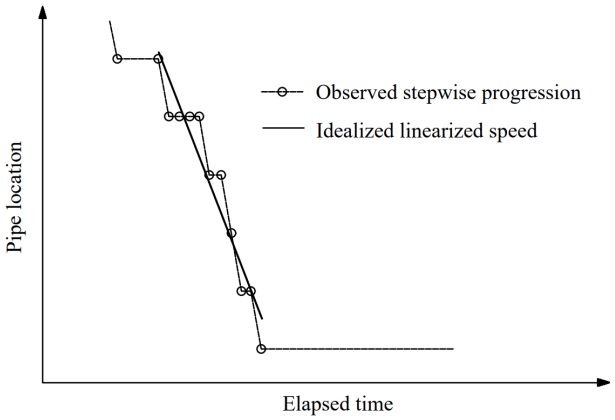

Fig. 2. Stepwise evolution of relative pipe location in a sand specimen with time in a laboratory erosion experiment (reproduced from data available in Robbins et al. (2018))

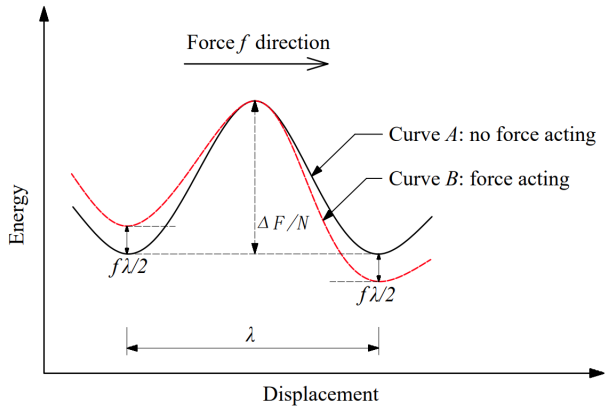

Fig. 3. Effect of a force on energy barriers (adapted from Mitchell & Soga (2005))

units to new positions requires expenditure of an activation energy ΔF to surmount the barrier (see Figure 2). The energy expended for a flow unit to cross a barrier may be provided by thermal energy and by various applied potentials. For a material at rest, the potential energy-displacement relationship is represented as curve A in Figure 3. The number of times that a given unit is activated, or the proportion of a certain number of flow units that are activated, v, per second is given by (frequency of activation):

$$v = \frac{k_b T}{h_p} \exp\left(-\frac{\Delta F}{RT}\right) \tag{1}$$

where, k_b is the Boltzmann's constant ($1.38 \times 10^{-23}\ J/K$), T is the absolute temperature (K), h_p is the Planck's constant ($6.624 \times 10^{-34}\ J/s$), and R is the universal gas constant ($8.3144\ J \cdot K^{-1} \cdot mol^{-1}$).

In the absence of directional potentials, flow units are oscillating across the barriers at equal frequency in all directions, generating no net directional flow. However, if a directed potential, such as a force, f, is applied, then the barrier heights are shifted as shown by curve B in Figure 3. The barrier height in the direction of the force is reduced and the activation frequency to the right is:

$$v \rightarrow = \frac{k_b T}{h_p} \exp\left(-\frac{\Delta F}{RT} + \frac{f\lambda}{2k_b T}\right) \tag{2}$$

and the frequency to the left is:

$$v \leftarrow = \frac{k_b T}{h_p} \exp\left(-\frac{\Delta F}{RT} - \frac{f\lambda}{2k_b T}\right) \tag{3}$$

where $R = k_b N$ and N is the Avogadro constant (6.022×10^{23}), and λ represents the distance between successive equilibrium positions. Therefore, the net frequency or probability of activation towards the direction of the force direction becomes:

$$(v \rightarrow) - (v \leftarrow) = 2\frac{k_b T}{h_p} \exp\left(-\frac{\Delta F}{RT}\right) \sinh\left(\frac{f\lambda}{2k_b T}\right) \quad (4)$$

This derivation in the context of studying shearing resistance of soils was originally conceived by Mitchell (1964). At any instant, the number of the flow units which are successful in crossing the energy barrier is obtained by the multiplication of the total number of flow units and the frequency/probability as defined in Eq. (4).

In this context, soils are described as assemblies of particles in equilibrium, with forces sustained and transferred thorough solid-to-solid contacts between adjacent particles (Mitchell, 1964). From the perspective of an individual particle, movement is prevented by several inter-particle contacts between neighbors. Erosion of soil particles involves two processes, displacement and transport, of the individual particles. It is postulated that, the former process requires relative movement primarily through sliding and/or rolling at inter-particle contacts, while the latter involves dilation of the soil structure when two adjacent particles must be pushed apart to create spaces for the displaced particles to move into. The postulated micro-structural process is similar to that derived in explanation of soil deformation, shearing resistance, and creep (Mitchell, 1964; Mitchell et al., 1968, 1969). Although the engineering phenomena of soil deformation, shearing resistance are different from the internal erosion process in BEP by definition, the underlying mechanism might all be attributed from relative displacements and rearrangements of soil particles. This might be an explanation of why these seemingly different processes have all been well described by the theory of rate processes. Further derivations of equations for computing erosion rate under hydraulic loading based on Eq. (4) are developed in the next section.

ANALYTICAL DERIVATION

In order to specialize the general rate process formulation presented above to the study of BEP, we first introduce the concepts of energy and power in the groundwater flow in a porous cohesionless medium. Several researchers have proposed the application of a flow energy to represent the hydraulic loading that initiates and maintains the internal erosion of soil particles, as an alternative to traditional methods employing the hydraulic gradient and hydraulic shear stress as a metric for erosion description (Gelet & Marot, 2022; Kodieh et al., 2021; Marot et al., 2012; Sibille et al., 2015). Marot et al. (2012) developed an energy analysis on internal erosion of cohesionless soils based on the energy conservation equation for the fluid phase. Details of this concept can be found in Marot et al. (2012), White (1999), and Sibille et al. (2015). Marot et al. (2012) proposed a measure of flow power to quantify the power carried by seepage flow which is expended for erosion. If a control volume of fluid flow is considered, through deductions based on the energy equations (White, 1999; Marot et al., 2012; Sibille et al., 2015), the flow power, P_{flow}, is given by:

$$P_{flow} = -\int_{S_i} (p\,\mathbf{v}\cdot\mathbf{n}_i + \gamma_w z\,\mathbf{v}\cdot\mathbf{n}_i)\,dS - \int_{S_o} ((p+\Delta p)\,\mathbf{v}\cdot\mathbf{n}_o + \gamma_w(z+\Delta z)\,\mathbf{v}\cdot\mathbf{n}_o)\,dS \quad (5)$$

where, S_i and S_o are the inlet and outlet boundary surfaces of the control volume; p and $p + \Delta p$ are the static pressures at the inlet and outlet boundary surfaces; z and $z + \Delta z$ are the elevations at the inlet and outlet boundary surfaces; $\mathbf{v}$ is the flow velocity; $\mathbf{n}_i$ and $\mathbf{n}_o$ are outer unit normal vector of the inlet and outlet boundary surfaces; and γ_w is the unit weight of water. There are five assumptions behind Eq. (5): (i) the energy is mainly dissipated by viscous shear at the direct vicinity of the solid particles, (ii) the fluid temperature is constant, (iii) the system is adiabatic, (iv) a steady-state flow is considered, and (v) the flow is considered laminar (Gelet & Marot, 2022; Marot et al., 2012). The first assumption states that most of the energy expenditure in the flow is on dissipation during solid-fluid interactions which directly contributes to erosion of soil particles. Sibille et al. (2015) demonstrated with results of laboratory internal erosion experiments that the energy expended on erosion may represent about 99 % of the flow energy in all cases. However, in the case of surface erosion, this approximation may not hold with a turbulent fluid flow (Bagnold, 1980; Govers, 1992).

The instantaneous cumulative expended flow energy at time t can be calculated by integrating the instantaneous flow power over time:

$$E_{flow}(t) = \int_t^{t+\Delta t} P_{flow}\,dt \quad (6)$$

Based on the previous, one can define the volumetric flow energy and power densities as $\bar{P}_{flow}(t) = P_{flow}(t)/V$, and $\bar{E}_{flow}(t) = E_{flow}(t)/V$, respectively ($V$ is the control volume). Then, according to Eq. (6), $\bar{E}_{flow}(t) = \int_t^{t+\Delta t} \bar{P}_{flow}\,dt$.

Energy-based constitutive relationships have been demonstrated as an advantageous approach to evaluate evolution of BEP in soils embankments (Kodieh et al., 2021). Therefore, in this study, we formulate a new constitutive model based on the flow energy concept and the theory of rate processes to describe the evolution of BEP.

At any instant, the total number of flow units per unit volume times the probability of crossing energy barriers as defined by Eq. (4) gives the number of flow units eroded by hydraulic loading per unit volume per unit time:

$$\frac{\partial \bar{n}}{dt} = 2\bar{n}\frac{k_b T}{h_p}\exp\left(-\frac{\Delta F}{RT}\right)\sinh\left(\frac{f\lambda}{2k_b T}\right) \tag{7}$$

where, $\bar{n}$ denotes the average number of flow units per unit volume. By virtue of the flow energy definition provided earlier, Eq. (7) can be rewritten as:

$$\frac{\partial \bar{n}}{dt} = 2\bar{n}\frac{k_b T}{h_p}\exp\left(-\frac{\Delta F}{RT}\right)\sinh\left(\frac{\bar{E}_{flow}V_f}{k_b T}\right) \tag{8}$$

where, V_f is the idealized average volume of a flow unit, as defined by Andersland & Douglas (1970) and Gularte et al. (1980). In Eq. (8), the adjustment of the height of the free activation energy, as shown in Figure 3, $f\lambda/2$ is replaced by $\bar{E}_{flow}V_f$, both referring to the energy expenditure on a given flow unit. Based on aforementioned discussions, the flow energy density from the fluid flow $\bar{E}_{flow}$ can be estimated through integration of the flow power density $\bar{P}_{flow}$ over the unit time. Equations (7) and (8) are based on two assumptions on the control volume: (1) all flow units take part in erosion and are equally likely to be activated, and (2) flow energy is uniformly distributed over the control volume.

Let m_{fu} denote the average mass of a flow unit. By multiplying m_{fu} on both sides, Eq. (8) becomes:

$$\frac{\partial \bar{n}}{\partial t}m_{fu} = 2\bar{n}m_{fu}\frac{k_b T}{h_p}\exp\left(-\frac{\Delta F}{RT}\right)\sinh\left(\frac{\bar{E}_{flow}V_f}{k_b T}\right) \tag{9}$$

The left-hand side of Eq. (9) represents the average mass erosion rate per unit volume which is denoted as $\dot{m}$ in this paper:

$$\frac{\partial \bar{n}}{\partial t}m_{fu} = \dot{m} : = \frac{\partial m}{\partial t}\frac{1}{V} \tag{10}$$

where, $\partial m/\partial t$ gives the rate of erosion of soil mass (in units of mass over time).

The term $\bar{n}m_{fu}$ on the right-hand side of Eq. (9), representing the total mass of flow units per unit volume, is equal to the total mass of solid matter of soil particles per unit volume which is usually defined as the dry bulk density of soil, ρ_{dry}.

Substituting $\dot{m}$ and ρ_{dry} into Eq. (9), one obtains:

$$\dot{m} = 2\rho_{dry}\frac{k_b T}{h_p}\exp\left(-\frac{\Delta F}{RT}\right)\sinh\left(\frac{\bar{E}_{flow}V_f}{k_b T}\right) \tag{11}$$

Mitchell et al. (1969) defined a parameter S as the idealized number of bonds per unit area, representing the number of interparticle bonds averaged over a unit area which is an important indicator of the soil structure. By assuming the separation distance between successive equilibrium positions constant, the flow volume V_f can be expressed as:

$$V_f = \frac{\lambda}{S} \tag{12}$$

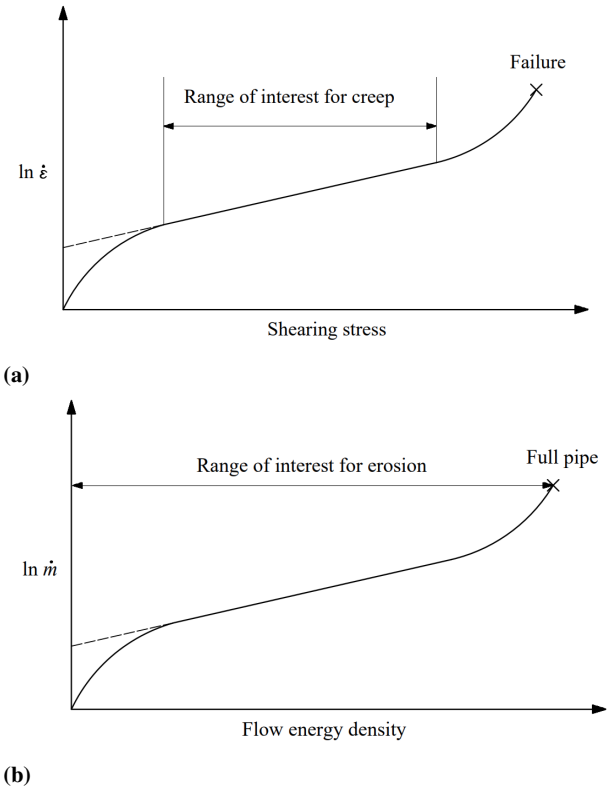

Fig. 4. Typical relationships between: (a) shearing stress and creep strain rate for a given time after start of creep, and (b) flow energy density and mass erosion rate per unit volume

where, according to Mitchell et al. (1969), a reasonable value of λ is assumed to be 2.8×10^{-10} m which is the diameter of an oxygen ion. This assumption is based on the relatively constant surface structure of silicate layers on soil particles, both in clay and sand. By substituting Eq. (12) into Eq. (11), we obtain:

$$\dot{m} = 2\rho_{dry}\frac{k_b T}{h_p}\exp\left(-\frac{\Delta F}{RT}\right)\sinh\left(\frac{\bar{E}_{flow}\lambda}{Sk_b T}\right) \tag{13}$$

Equation (13) provides a constitutive relationship between the flow energy density and the erosion rate per unit volume, which follows a hyperbolic sine relationship. The dry bulk density, ρ_{dry}, and absolute temperature T can be measured from the soil sample and k_b, R, and h_p are known constants. Therefore, only two parameters need calibration to derive the constitutive equation, i.e., the activation energy ΔF, and the number of flow units per unit area S.

In the literature, the hyperbolic sine in Eq. (4) has been often approximated as an exponential (Mitchell, 1964; Mitchell et al., 1969; Gularte et al., 1980). Mitchell (1964) argued that in the range of shearing stress of engineering interest, it suffices that $f\lambda/2kT > 1$ so that the hyperbolic sine can be approximated as exponential with reasonable accuracy. This approximation is well illustrated by the typical strain rate-shear stress curve at a given time after start of creep obtained from soil creep experiments as shown in Figure 4a. The cases when the shearing force f is too small to satisfy this condition were

not considered. However, in the study of erosion, this kind of approximation can not be adopted on Eq. (13), because when the flow energy is small and the approximation cannot be made, BEP may be initiating, making this portion of the curve of great importance (see Figure 4b). Therefore, in this study, the hyperbolic sine in Eq. (13) is kept as per the mathematical derivations presented earlier:

$$\dot{m} = \alpha \, \sinh\left(\beta \, \bar{E}_{flow}\right) \tag{14}$$

where the following substitutions were made for convenience:

$$\alpha = 2\rho_{dry} \frac{k_b T}{h_p} \exp\left(-\frac{\Delta F}{RT}\right) \tag{15}$$

and,

$$\beta = \frac{\lambda}{S k_b T} \tag{16}$$

Equation (14) is a two-parameter relationship which may be capable of describing the flow energy intensity-erosion rate characteristics of different soils. Under a given temperature, the parameter α is a function of the dry bulk density ρ_{dry} and the activation energy ΔF of the soil, the former of which can be easily measured. The parameter β is a function of the number of bonds per unit area, S. For a soil under study, several internal erosion tests are required to establish the values of α and β while maintaining a constant temperature and confining stress for all tests, through non-linear regression analysis on experimental data.

PRELIMINARY INVESTIGATION WITH EXPERIMENTAL OBSERVATIONS

The constitutive relationship derived in the previous (see Eq. (14)) is first exercised to quantitatively characterize the values of free energy of activation ΔF and the number of bonds per unit area S from internal erosion experimental data from the literature. This comparison is used as a basis to evaluate the observed range of the two parameters, and shed light on the applicability of rate process theory to internal erosion mechanisms. Data from four different internal erosion tests with measurements of mass erosion rates are analyzed. Specifically, Riha & Petrula (2023) performed BEP experiments on sand samples in a box with a 120 $mm \times$ 120 mm cross section and a 350 mm erosion path. The testing apparatus and procedures employed in the suffusion experiments reported in (Sterpi, 2003; Sail et al., 2011; Marot et al., 2012) are similar with cylindrical sand samples confined in rigid cells. The test parameters used in the study are summarized in Table 1. Detailed information on the tested materials is given in Table 2. The seepage direction is downward in the experiments conducted by Sail et al. (2011) and Marot et al. (2012), whereas an upward seepage direction in the experiment was reported by Sterpi (2003). Marot et al. (2012) carried out tests in a geotechnical centrifuge and

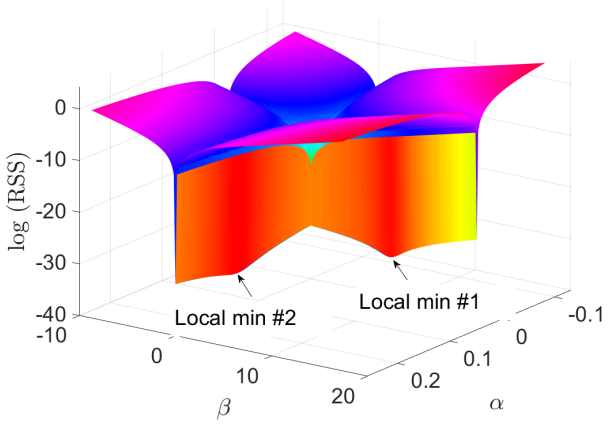

Fig. 5. Topology of RSS from regression analysis on data available in Marot et al. (2012), RSS at local min #1: 2.5×10^{-33}**, RSS at local min #2:** 1.3×10^{-33}

different sample lengths were used. Constant vertical surcharge loads of 25 kPa and 14.2 $\sim$ 42.5 kPa were applied during the experiments carried out by Sail et al. (2011) and Marot et al. (2012), respectively. In each experiment, prescribed hydraulic loading was applied to the specimens through hydraulic control components, while the eroded mass and flow rates were measured. The flow energy at any instant can be computed from the applied hydraulic gradient and flow rate measurements from Eqs.(5) and (6). Temperatures were not reported or controlled in these experiments. Since temperature plays an important role in the theory of rate processes, the results of experiments and the analysis below could be affected if temperatures were controlled during the experiments.

The parameters α and β in Eq. (14) are estimated through non-linear regression on the experimental data (Teunissen, 1990). Figure 5 reports the topology of the objective function (i.e., the residual sum of squares (RSS) on the observations) from one dataset for the non-linear regression analysis carried out. For each case, two local minima are detected from the 3D plots and are labeled as “local min #1” and “local min #2”, respectively. Therefore, as shown in Figure 6, on each dataset, two separate non-linear least-squares regressions were performed with initial values of α and β corresponding to the two local minima to obtain accurate estimates of α and β. A 95% confidence interval was plotted together with each nonlinear regression curve. Nonlinear regression NL1 (corresponding to local min #1) predicts that erosion rate accelerates with at lower flow energy densities (when $\bar{E}_{flow} >$ 25 J/m^3 for Riha & Petrula (2023), $\bar{E}_{flow} > 3$ J/m^3 for Sail et al. (2011), and $\bar{E}_{flow} > 0.1$ J/m^3 for Sterpi (2003) and Marot et al. (2012)), whereas nonlinear regression NL2 (corresponding to local minimum #2) predicts that acceleration in erosion rate occurs at higher flow energy levels outside the range observed in the experiments. The dataset from Riha & Petrula (2023) contains a much larger amount of data and covers a wider range of flow energy densities, up to 40 J/m^3.

Table 1. Testing parameters of datasets reported in the literature

Reference	Type of test	Specimen dimensions (mm)	Global hydraulic gradient	Vertical surcharge load (kPa)	Centrifuge acceleration factor (g)
Riha & Petrula (2023)	BEP	Box: $350(L) \times 120 \times 120$	$0.75 \sim 1.80$	/	/
Sail et al. (2011)	Suffusion	Cylinder: $250 \sim 600(H) \times 280(D)$	$1 \sim 3$	25	/
Sterpi (2003)	Suffusion	Cylinder: $140(H) \times 70(D)$	$0.18 \sim 0.75$	0	/
Marot et al. (2012)	Suffusion	Cylinder: $60 \sim 120(H) \times 73(D)$	$45 \sim 150$(scaled)	$14.2 \sim 42.5$	$13.3 \sim 40$

Table 2. Description of tested materials

Reference	Components	Void ratio	Dry bulk density (g/cm^3)	Particle size, D_{50} (mm)	Uniformity coefficient, C_u	Gradation
Riha & Petrula (2023)	Three medium sands: grain size $0/2mm$	$0.40 \sim 0.62$	$1.63 \sim 1.88$	$0.63 \sim 1.13$	$1.84 \sim 2.98$	Uniform
Sail et al. (2011)	Mixture of glass beads: 40% small + 60% large	0.36	1.84	1.42	14.43	Gap graded
Sterpi (2003)	Recovered Milano natural sand	0.51	1.80	0.36	39.32	Well graded
Marot et al. (2012)	Clayey sand: 90% Fontainebleau sand + 10% kaolinite clay	0.42	1.91	0.20	2.49	Poorly graded

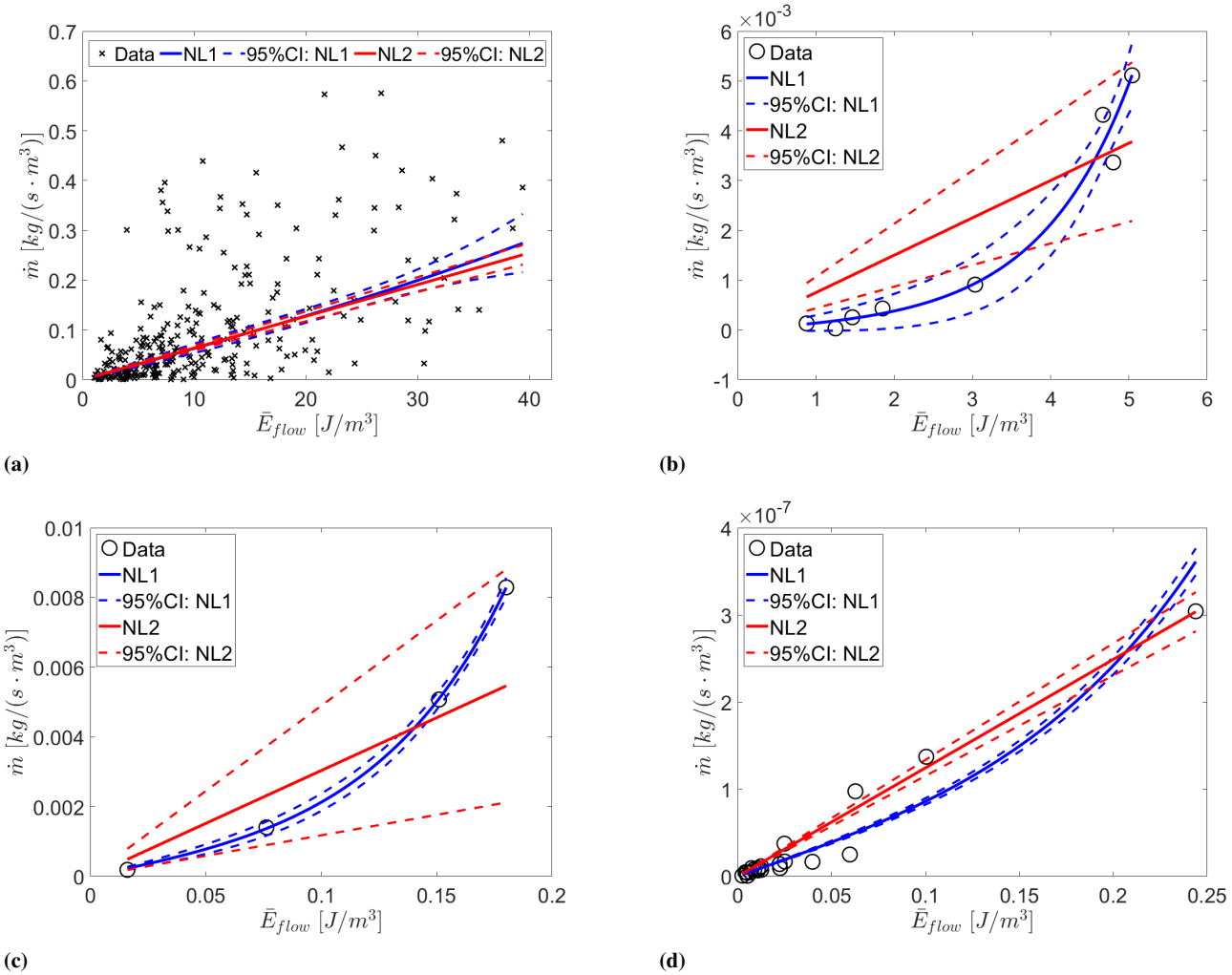

Fig. 6. Nonlinear regression on data obtained from: (a) BEP experiments in Riha & Petrula (2023), and suffusion experiments in (b) Sail et al. (2011), (c) Sterpi (2003), and (d) Marot et al. (2012)

Interestingly, the erosion rates predicted by the two regression curves on the data from Riha & Petrula (2023) (Fig. 6(a)) show a much more consistent trend (with respect to each other) when compared to the other selected internal erosion tests. Moreover, in the observations of Marot et al. (2012), there is no evidence that erosion rate is accelerating, unlike Sail et al. (2011) and Sterpi (2003); this difference is especially obvious in the data from Sterpi (2003) as the flow energy density magnitudes are similar to Marot et al. (2012). The higher-valued datapoints in small flow energy density regime are very well captured with the NL2 parameters for Sterpi (2003) and Marot et al. (2012) datasets. At higher flow energy density values ($> 0.15\ J/m^3$), the two experiments appear to differ in their behavior; Sterpi (2003) shows acceleration in mass loss and Marot et al. (2012) does not. For regression with the BEP data in Riha & Petrula (2023), the 95% confidence intervals of NL2 is narrower than that of NL1 at higher flow energy density, indicating higher plausibility of NL2 in this case. For suffusion data from Sail et al. (2011) and Sterpi (2003), the 95% confidence intervals of NL1 are narrower than those of NL2, while for the data from Marot et al. (2012) the interval widths of two regressions are similar. With the regression analysis, we cannot conclude which of the two regressions is more representative of the true behavior of the soil for prediction purposes. Notwithstanding the significant differences between the reported tests, both in terms of testing conditions and materials, the results demonstrate that the estimated values of ΔF and S fall within a consistent range, highlighting how the theory of rate processes can describe internal erosion mechanisms. The obtained results, in terms of activation energy and number of bonds, represent the basis for the BEP investigations proposed in the following.

Activation Energy Measures

The calculated activation energy values, along with those reported in the literature, are summarized in Table 3. The values for the activation energy from the selected datasets are $96.9 \sim 134.6\ kJ/mol$ and $74.9 \sim 97.0\ kJ/mol$ as estimated from NL1 and NL2, respectively. Values from both regressions fall into the range of measurements from creep and surface erosion experiments reported in the literature (Andersland & Douglas, 1970; Christensen & Das, 1973; Gularte et al., 1980; Mitchell et al., 1969; Murayama et al., 1984). The estimated activation energy values from NL1 in this study are close to those reported for creep (Andersland & Douglas, 1970; Mitchell et al., 1969; Murayama et al., 1984), and are higher than those reported from surface and hole erosion tests (Christensen & Das, 1973; Gularte et al., 1980). On the other hand, the activation values from NL2 on the internal erosion data are closer to those from surface erosion tests and lower than creep.

According to the discussions above, activation energy ΔF represents the energy expenditure to activate one mole of flow unit. Mitchell & Soga (2005) hypothesized that movement of each soil particle requires rupture of single solid-to-solid bonds or simultaneous rupture of several such bonds between soil particles at contact. Physical evidence for presence of solid-to-solid contacts and interparticle bonds has been obtained in both clays and sands (Albalasmeh & Ghezzehei, 2014; Matsui et al., 1980). Furthermore, Mitchell & Soga (2005) proposed that the cause of creep movements of soil particles and rupture of interparticle bonds is due to slow diffusion of oxygen ions in and around interparticle contacts. This interpretation accounts for the features of the estimated values of the activation energy from previously reported results: (1) the activation energy values fall into the range of chemical reactions ($40 \sim 400\ kJ/mol$); (2) the magnitude of the activation energy does not vary much with changes in water content, consolidation pressure, and void ratio; and (3) the values of activation energy are similar for both sands and clays. This postulate is somehow consistent with the fact that the calculated values of activation energy from this study are of similar magnitudes themselves and fall within the range of previously reported estimates, even though the type of experiments and soils are significantly different than the previously described research.

Number of Bonds Per Unit Area

Table 4 reports the estimated number of bonds per unit area, along with those reported in the literature. The values estimated herein are $0.41 \times 10^{10} \sim 3.25 \times 10^{12}$ and $0.42 \sim 7.81 \times 10^{16}$ from NL1 and NL2, respectively. The values from NL1 are slightly larger than those estimated from surface erosion tests (Gularte et al., 1980; Christensen & Das, 1973), four to five orders of magnitudes smaller than those reported for creep by Mitchell et al. (1969), and about ten orders of magnitudes smaller that of Andersland & Douglas (1970) for creep. The computed numbers of bonds per unit area in this study with NL2, however, are six orders of magnitudes larger than those from NL1.

Mitchell et al. (1969) studied the relationships between number of bonds per area, effective stress, and strength of different soils. From their study, the number of bonds is shown to be proportional to the magnitude of the effective stress, and the strength of a soil is found to be directly proportional to the number of these bonds. The same proportionality between the number of bonds and the soil strength holds for both clay and sand. Furthermore, Mitchell et al. (1969) showed that at any value of effective stress, the number of bonds per area is about the same for sand and clay, independent of particle size. A plausible physical interpretation for these experimental results is proposed by Mitchell & Soga (2005) stating that the bonds are possibly of the primary valence type formed between oxygen atoms and silicon atoms at interparticle contacts that transmit the effective stress. Mitchell & Soga (2005) further assumed that the number of bonds formed at a single contact is proportional to the effective stress transmitted through the contact. Michalowski et al. (2018) characterized surface texture of silica sand grains and visualized inter-granular contacts composing of many microscopic “contact

Table 3. Values of activation energy estimated from various studies

Material	Type of test	Activation energy (kJ/mol)	Reference
Medium sand	Internal erosion, BEP	96.9^{a} / 79.1^{b}	This study(data based on Riha & Petrula (2023))
Mixed glass beads	Internal erosion, suffusion	116.0^{a} / 77.1^{b}	This study(data based on Sail et al. (2011))
Milano sand	Internal erosion, suffusion	111.6^{a} / 74.9^{b}	This study(data based on Sterpi (2003))
Clayey sand	Internal erosion, suffusion	134.6^{a} / 97.0^{b}	This study(data based on Marot et al. (2012))
Grundite, remoulded	Surface erosion	$72.8 \sim 107.0$	Gularte et al. (1980)
Grundite	Hole erosion	64.5	Christensen & Das (1973)
Kaolinite	Hole erosion	68.2	Christensen & Das (1973)
Sault St Marie clay	Creep	117	Andersland & Douglas (1970)
Osaka clay, normally consolidated	Creep	$120 \sim 134$	Murayama & Shibata (1961)
Illite, remoulded	Creep	$105 \sim 165$	Mitchell et al. (1969)
Illite, dry	Creep	155	Mitchell et al. (1969)
San Francisco Bay mud, undisturbed	Creep	$105 \sim 135$	Mitchell et al. (1969)
Sacramento River sand, dry	Creep	105	Mitchell et al. (1969)

Note: ^{a}estimated from regression NL1; ^{b}estimated from regression NL2.

Table 4. Values of number of bonds per unit area from various studies

Material	Type of test	Number of bonds per unit area (m^{-2})	Reference
Medium sand	Internal erosion, BEP	$3.25 \times 10^{12\ a}$ / $0.42 \times 10^{16\ b}$	This study(data based on Riha & Petrula (2023))
Mixed glass beads	Internal erosion, suffusion	$8.01 \times 10^{10\ a}$ / $7.81 \times 10^{16\ b}$	This study(data based on Sail et al. (2011))
Milano sand	Internal erosion, suffusion	$0.41 \times 10^{10\ a}$ / $0.45 \times 10^{16\ b}$	This study(data based on Sterpi (2003))
Clayey sand	Internal erosion, suffusion	$0.77 \times 10^{10\ a}$ / $1.66 \times 10^{16\ b}$	This study(data based on Marot et al. (2012))
Grundite, remoulded	Surface erosion	$0.46 \sim 1.82 \times 10^{9}$	Gularte et al. (1980)
Grundite	Hole erosion	3.45×10^{9}	Christensen & Das (1973)
Kaolinite	Hole erosion	5.75×10^{9}	Christensen & Das (1973)
Sault St Marie clay	Creep	1.65×10^{20}	Andersland & Douglas (1970)
Illite, remoulded	Creep	$3 \sim 20 \times 10^{14}$	Mitchell et al. (1969)
Illite, dry	Creep	5×10^{16}	Mitchell et al. (1969)
San Francisco Bay mud, undisturbed	Creep	$2 \sim 10 \times 10^{14}$	Mitchell et al. (1969)
Atioch sand, dry	Creep	$4 \sim 20 \times 10^{14}$	Mitchell et al. (1969)

Note: ^{a}estimated from regression NL1; ^{b}estimated from regression NL2.

points" with scanning electron microscopes (SEM). Wang (2017) demonstrated force transmission mechanisms at intergranular contacts through microscopic contact points with discrete element modeling (DEM).

Remark: The erosion model under investigation was developed from fundamental granular physics in the context of simulating BEP through the theory of rate processes, which has been proven capable of describing various processes in sands, such as surface and hole erosion. The main reason why both BEP and suffusion test data are included in this section is to show that the activation energy and number of bonds estimated through the model provide values that are reasonably similar for both cases and fall into the ranges reported in the literature. This is an interesting finding, because it opens up possibilities for a more fundamental understanding of internal erosion phenomena, based on the microgranular effects described through the theory of rate processes. At the same time, the authors remark that the proposed model was developed to describe backward erosion piping, therefore no claim is made to its capability to simulate suffusion. However, the authors believe that the fundamental description of internal erosion mechanisms as rate processes might be of value to other research groups that might use the theoretical framework developed herein and extend it to suffusion (based on the observation that the estimated parameters fall within a narrow range).

NUMERICAL INVESTIGATIONS ON BEP PROGRESSION

The constitutive relationship proposed in this study is evaluated by incorporating it into a multiphase numerical

model. Numerical simulations temporal BEP progression are conducted within this framework, and the results are compared with experimental findings obtained from the literature, to serve as calibration and validation. In particular, the calibrated values of activation energy and number of bonds are compared with those estimated from the regression analysis presented in the previous section and the values reported for surface erosion, hole erosion and creep in the literature. Sensitivity analysis is performed on different modeling parameters to study their influence on the simulation results.

Model Implementation

As originally presented in (Fascetti & Oskay, 2019a), the groundwater flow during the erosion process in the embankment is idealized using a nonlinear diffusion equation:

$$\frac{\partial h(x,t)}{\partial t} = \nabla \cdot (D(x,t))\, \nabla h(x,t) \quad x \in \Omega,\ t \in (0,T) \tag{17}$$

where, $h(x,t)$ represents the hydraulic head field, Ω is the computational domain, T is the total time, and $D(x,t)$ is the diffusivity coefficient of the soil:

$$D(x,t) = \frac{k(x,t)}{S_s} \tag{18}$$

where, $k(x,t)$ is the soil conductivity and S_s is the specific storage of the soil.

The computational domain is subject to the following boundary conditions:

$$h = h_b(t) \qquad on\ \ \Gamma_b \subset \partial\Omega \tag{19}$$

$$q \equiv -D\frac{\partial h}{\partial x} = q_b \qquad on\ \ \Gamma_q \subset \partial\Omega \tag{20}$$

with $\Gamma_b \cap \Gamma_q = \emptyset$. q is the outward flux, q_b is the prescribed boundary flux, and h_b the time-dependent prescribed hydraulic head at the boundary.

The mass balance equation for the fluidized particles reads:

$$\frac{\partial\left(\gamma(x,t)\phi(x,t)\right)}{\partial t} + \frac{\partial\left(\gamma(x,t)q(x,t)\right)}{\partial x} = \frac{\partial\phi(x,t)}{\partial t} \tag{21}$$

where, $\gamma(x,t)$ is the concentration of soil particles fluidized by the erosion process (i.e., the ratio between the volume of fluidized particles and the total volume of the fluid), and $\phi(x,t)$ is the soil porosity. It is worth mentioning that a limit porosity criterion is enforced in the simulations to guarantee numerical stability. Such value represents the maximum local porosity attained for fully piped conditions (i.e., $\phi(x,t) \leq \phi_{lim}$, with ϕ_{lim} being a model parameter). Based on its definition, such limit porosity is inherently different from the average maximum porosity measured from standard testing procedures (e.g., ASTM (2016)), which represents the average porosity of a soil sample in its loosest condition.

Recalling Eq. (10), the right-hand side of Eq. 21 can be written as:

$$\frac{\partial\phi(x,t)}{\partial t} = \frac{\dot{m}}{\rho_s} \tag{22}$$

where ρ_s is the density of soil particles. By substituting the constitutive relationship given in Eq. (14) into Eq. (22):

$$\frac{\partial\phi(x,t)}{\partial t} = \frac{1}{\rho_s}\alpha\ \sinh\left(\beta\ \bar{E}_{flow}(x,t)\right) \tag{23}$$

With the governing equations introduced above, a typical 1-D erosion problem was simulated. To solve the system of equations, the response field is discretized along the one-dimensional domain represented by the erosion path. Discretization in space is performed by means of a central finite difference scheme, while time is discretized by means of the Crank-Nicolson algorithm. The modeling procedure is as follows:

(i) Define and discretize the computational domain, assign initial values for the modeling parameters and boundary conditions. A higher local hydraulic gradient arises at the downstream exit area;

(ii) At every time increment, hydraulic head in the domain is computed through Eq. (17), and the hydraulic gradient is calculated. Compute flux with Darcy's law and porosity evolution rate with the constitutive relationship Eq. (23), with the computed hydraulic gradient and the conductivity. In practice, a threshold gradient value is often observed below which soil mass erosion either does not initiate or mass loss is too small to cause change in porosity (e.g., Robbins et al. (2018)). In these cases, a threshold gradient is used to calculate a cutoff flow energy density which is subtracted from the flow energy density values used in the computation;

(iii) Compute concentration of fluidized particles from the mass balance Eq. (21), update conductivity using Kozeny-Carman equation, and update diffusivity. The simulation continues until the target total time or number of iterations is met. In case the initial state provided in Step (i) does not introduce a local gradient that exceeds the critical value, the solution is trivial and piping does not progress through the domain.

Experimental Works Simulated

The multiphase numerical framework described in the previous is used to simulate the BEP experiments reported in Robbins et al. (2018), Vandenboer et al. (2019), and Pol et al. (2022). In the BEP experiment performed by Robbins et al. (2018), a sand sample with a 958 mm erosion path was tested in an acrylic cylinder with an internal diameter of 76.2 mm, with a free slope exit condition at the downstream end. In Vandenboer et al. (2019) and Pol et al. (2022), sand samples were tested in boxes with lengths of erosion path of 352 mm and 300 mm, respectively, a width of 300 mm and a height

Table 5. Calibration of model parameters in 1-D erosion simulation with data obtained from: R-Test 7B in Robbins et al. (2018), V-Test with gradual loading in Vandenboer et al. (2019), and P-Test FPH_237 in Pol et al. (2022)

Parameter	R	P	V
Length of erosion path (mm)	958	352	300
Global and threshold gradient	0.41	0.19	0.20
Initial porosity	0.379	0.399	0.403
Hydraulic conductivity ($10^{-4}m/s$)	6.20	1.10	1.03
Limit porosity	0.624^c	0.549^c	0.549
Specific storage ($10^{-5}m^{-1}$)	7.20^c	7.57	7.64
Activation energy ΔF (kJ/mol)	73.70^c	73.70	73.70
Number of bonds S ($10^{13}m^{-2}$)	6.76^c	9.92^c	12.65^c

Note: ^{c}calibrated with experimental results.

of 100 mm; the samples were covered by an acrylic lid with an exit hole downstream. In these experiments, the progression rates of piping were monitored through timestamped video data, and local hydraulic heads were measured during the tests through pressure gauges installed along the erosion paths. While the setup of the experiments from Robbins et al. (2018) and Pol et al. (2022) were designed to produce a 1-D erosion path for convenient gradient measurements, the test setup in Vandenboer et al. (2019) was designed to resemble more realistic 3-D conditions.

Simulation Results

The model parameters used in all the reported simulations are summarized in Table 5. The values of activation energy and number of bonds estimated from the regression analyses presented in the previous section were employed as initial values for the calibration. Based on the discussion and theoretical derivations, activation energy is viewed as an intrinsic property of soils, therefore its value was calibrated from the experiment performed by Robbins et al. (2018) and maintained constant in all the other simulations. The threshold gradients used for the calculations are the same as the global average gradients. This choice was made to provide consistency with the reported experimental results, which also include information on global gradients. The limit porosity values were also calibrated from the experimental data. The limit porosity value that was calibrated from Pol et al. (2022) data was employed in the simulation for the test from Vandenboer et al. (2019), since the soils tested in these experiments were similar. Similarly, the value of specific storage in the simulation of experiment from Robbins et al. (2018) was first calibrated. Based on the calibrated specific storage value, the power law relationship proposed by Kuang et al. (2020) was employed to evaluate specific storage values in the simulations of the tests

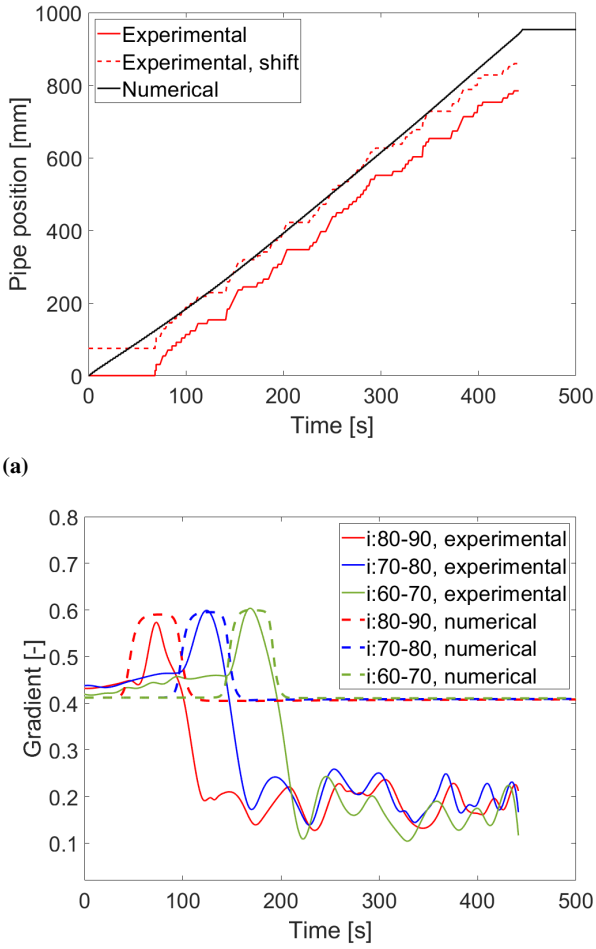

Fig. 7. Comparisons of simulation results and experimental data: (a) pipe progression rate, and (b) evolution of local gradients (experimental data available in Robbins et al. (2018))

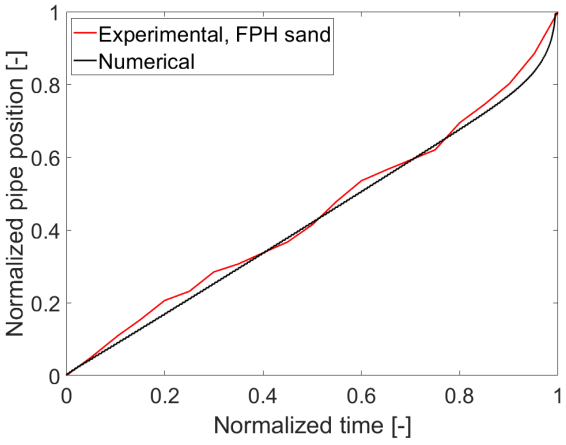

Fig. 8. Calibration of model with BEP experimental data from Test FPH_237 in Pol et al. (2022)

reported by Vandenboer et al. (2019) and Pol et al. (2022). As illustrated by Table 5, the values of number of bonds per unit area S calibrated with observations from independent BEP experiments with different sands fall into the range of values reported in literature for various mechanisms (see Table 4).

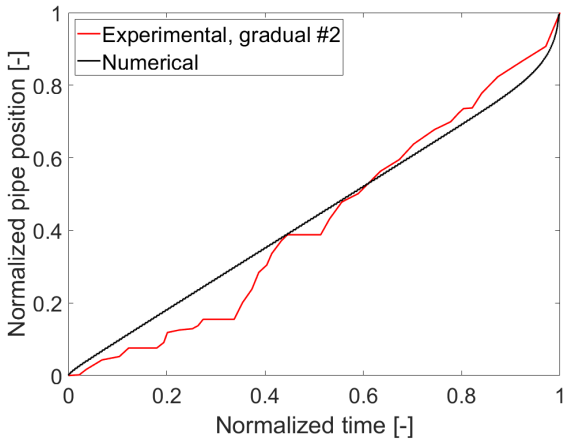

Fig. 9. Calibration of model with BEP experimental data from Test gradual#2 in Vandenboer et al. (2019)

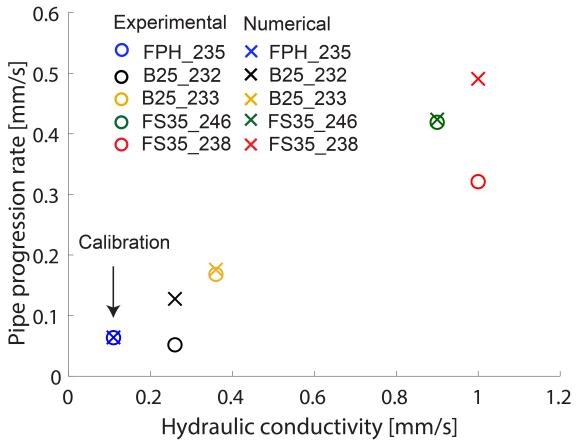

Fig. 10. Validation of simulation results with data from BEP experiments (data in Pol et al. (2022))

These results further demonstrate the capability of the proposed constitutive model of describing BEP at a fundamental level.

Figure 7 reports the comparison of the simulation results with the experimental observations from Robbins et al. (2018) in terms of pipe progression rate (Fig.7(a)) and the evolution of local hydraulic gradients (Fig.7(b)). The comparison between numerical and experimental pipe progression rates was employed as a means to calibrate the model parameters, as reported in Table 5. A satisfactory agreement is achieved in the average pipe progression rate and both numerical and experimental curves exhibit a relatively constant progression rate during the whole process. It is worth noting that in the comparison the experimental curve was shifted by 70 mm to account for the difference in identification of the pipe tip in the experiments, when compared to the numerical results. A significant difference between the experimental and simulation outcomes that can be observed in Fig. 7(a) is in the step size of pipe progression; the pipe progressed in non-uniform steps during the experiment, whereas in uniform and smaller steps in the simulation. Two idealizations in the simulation might have contributed to this behavior: (a) the time resolution is much higher in the numerical simulation than the measurement frequency in the experiment, and (b) the diffusion equation Eq. (17) might smooth out local spatial heterogeneity of seepage flow which are inherently present in the experiments (Powell & Richerson, 1985).

Figure 7(b) shows the comparison of the evolution of local hydraulic gradients during the experiment, demonstrating an excellent agreement. It is worth highlighting that the simulation with model parameters calibrated using the pipe progression rate successfully reproduced the evolution of local gradients observed in the experiment. This cross-validation from two independent features observed in the experiment provides supporting evidence for the validity of the proposed approach. The observed local gradients further dropped to the range of $0.10 \sim 0.25$ after the pipe tip passed through, whilst the simulation results show that the local gradients fell back to the initial value of 0.41 after the passage of the pipe. One possible explanation for this discrepancy is that, during the experiment, once the pipe had progressed entirely through the sample, the upstream hydraulic head was no longer maintained constant, causing a decrease in the value of the head at the upstream side and consequently in the hydraulic gradient. Conversely, the upstream and downstream hydraulic heads were maintained constant throughout the simulation. Since the further drop in gradients were also observed in other experimental works(e.g., in Pol et al. (2022)), another explanation is that the resistance to seepage flow in the pipe is much lower than in the soil. Moreover, a sudden step forward in pipe progression as observed in the experiment might have contributed to the different heights between the first gradient peaks in the experimental and numerical data in Fig. 7(b). By a closer look at both Figs. 7(a) and 7(b), the first gradient peak happened at about 70 sec when the pipe location experienced a sudden step forward. Robbins et al. (2018) pointed out that when pipe progressed rapidly through the sample, the hydraulic conditions were likely not near equilibrium, which might be the reason for the lower height of the first peak in the gradient. On the other hand, during the simulation, hydraulic equilibrium of the model was ensured by choosing stable computational time step when applying the Crank-Nicolson method (Fascetti & Oskay, 2019a; Thomas, 2013). Overall, the good agreement on both pipe progression rates and the evolution of local gradients demonstrates the capability of the multiphase model in capturing the main hydraulic conditions in the soil during BEP progression.

Figures 8, 9 and 10 illustrate calibration and validation of the model with data from backward erosion piping experiments performed by Vandenboer et al. (2019) and Pol et al. (2022). The model parameters for the test in Pol et al. (2022) were calibrated with the pipe progression rate measured from Test FPH_237, with a global hydraulic gradient of 0.19 and an average pipe progression rate of 0.064 mm/s. As shown in Fig.8, the model is capable of replicating the experimental pipe progression curve. Once the model parameters were calibrated,

four other experiments with two types of different sands and different hydraulic conductivity values were employed for validation, as shown in Fig.10. The increasing trend of pipe progression rate with increasing hydraulic conductivity, which was demonstrated in Pol et al. (2022), is well captured by the model. Discrepancies exist between the validation data points with hydraulic conductivity values of 0.26 mm/s and 1.00 mm/s, for which the measured progression rates are lower than those predicted by the simulations. This difference could be ascribed to the variability in testing conditions and soil properties within the samples in the various experiments, as BEP has been demonstrated to be highly sensitive to spatial variation in soil properties by Negrinelli et al. (2016).

Sensitivity Analysis

A sensitivity analysis was performed to assess the effect of the different model parameters on the simulation results. In particular, the sensitivity to the meshing resolution, coefficients of the hyperbolic sine constitutive law, initial diffusivity, and limit porosity of the sand specimen was investigated. A one-at-a-time (OAT) method was employed for the sensitivity analysis, which analyzes the effect of one parameter on simulation results at a time while keeping the others fixed (Saltelli et al., 2008). The outcome of simulations with different mesh densities is given in Figure 11. The simulation results of the general trend of pipe progression were not affected by the mesh density except for a variation in the step sizes of pipe propagation, which derives from the different spatial resolution. Therefore, when step sizes are not a concern, a high mesh density is not necessary to save simulation time and computational resources. The sensitivity of the simulation results to the coefficients of the hyperbolic sine constitutive law, initial diffusivity, and limit porosity of the sand specimen is summarized in Fig. 12. The sensitivity is illustrated as the variation of the normalized average velocity of pipe progression with respect to changes of the model parameters under exam. The normalized average velocity of pipe progression is defined as the average velocity of pipe progression, which equals to the sample length divided by time for formation of a full pipe, divided by the average velocity of pipe progression computed with the original parameters in Table 5. As shown in Fig. 12, the pipe progression speeds up with increase of all the four parameters under study. For smaller parameter values (i.e., normalized values smaller than 1), the simulation results are more sensitive to the limit porosity, followed by the hyperbolic sine coefficients, and are the least sensitive to the initial diffusivity. For larger parameter values (i.e., normalized values larger than 1), the sensitivity of the model to both the initial diffusivity and the limit porosity decreases, while the sensitivity to the two hyperbolic sine coefficients is generally higher, as expected. In the range of variation considered herein (0.6∼1.4), the effects of changes in the two hyperbolic sine coefficients are similar, and the velocity of pipe progression

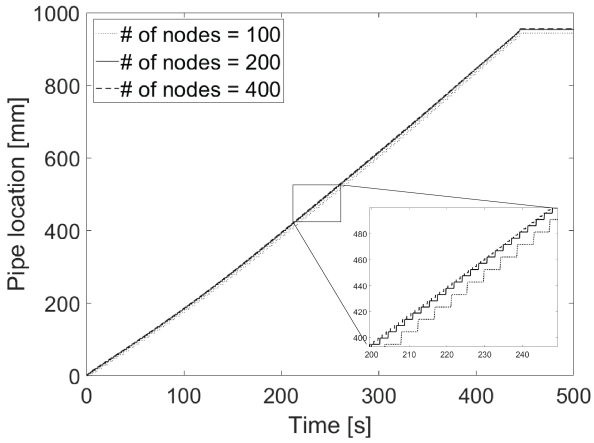

Fig. 11. Influence of the meshing resolution on the simulated pipe progression

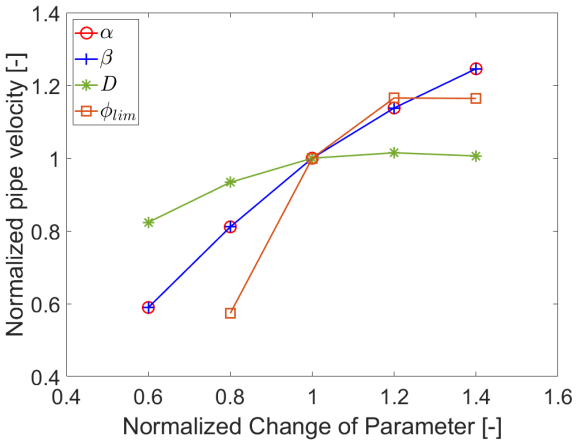

Fig. 12. Influence of the model parameters on the simulated time to development of full pipe

changes approximately in a linear fashion with changes in each of these two parameters.

DISCUSSION ON SIMULATION RESULTS

The model parameters ΔF and S calibrated from the comparisons with the BEP experimental results are equal to 73.70 KJ/mol and 6.76 $\sim$ 12.65 $\times 10^{13}$ m^{-2}, respectively. Referring to the values listed in Tables 3 and 4, the estimated activation energy values and numbers of bonds per unit area from NL2 are more plausible according to the following reasoning: (1) estimated values of activation energy are in good agreement with those calibrated from the simulations, as hypothesized during model development; (2) the values for the number of bonds calibrated from the simulations are consistent with those obtained from NL2, by taking into account the influence of the effective stress in the soil Mitchell et al. (1969), as the sand specimens in Robbins et al. (2018), Vandenboer et al. (2019), and Pol et al. (2022) were tested without applying surcharge loads. Moreover, during the experiments progressive pipes were visualized in the samples, which means, according to Fleshman & Rice (2014), a loosened zone being present

in the vicinity of the pipe tip. Fleshman & Rice (2014) have shown that this loosened zone has a greater porosity and, therefore, a smaller average effective stress. Additionally, the samples in Sail et al. (2011) and Marot et al. (2012) were tested under surcharge loads of $14 \sim 43\ kPa$, which yielded greater effective stresses in the samples as discussed in the previous. Therefore, it is likely that the average effective stresses in the loosened zone in the soil samples in the BEP experiments were smaller than those in the samples of the other suffusion experiments, but at the same time be expected to be larger than that of the hole and surface erosion tests reported in Christensen & Das (1973) and Gularte et al. (1980), in which soil particles were eroded from a free surface. Consequently, it is reasonable that the values of number of bonds per unit area calibrated from the simulations ($6.76 \sim 12.65 \times 10^{13}\ m^{-2}$) fall between those from the suffusion tests ($\sim 10^{15}$ to 10^{16}) and surface/hole erosion tests ($\sim 10^{9}$). The number of bonds per unit area estimated from data available in Sterpi (2003) is smaller than those from the other two datasets. This is likely due to the same reasoning, since the samples in this set of tests were not loaded.

Comparing the calibrated values of activation energy and numbers of bonds per area with those reported for surface erosion, hole erosion and creep in the literature (refer to Tables 3, 4, and 5), variations may be explained based on the proposed constitutive model. Should the postulates of Mitchell et al. (1969) and Mitchell & Soga (2005) on activation energy and number of bonds per unit area be accepted, values of activation energy would not vary significantly with either types of soil or testing conditions, and numbers of bonds per unit area should remain proportional to the effective stresses. The calibrated value of activation energy from from the BEP datasets ($73.7\ KJ/mol$) falls into the range of those from surface/hole erosion tests ($65 \sim 107\ KJ/mol$), but are significantly lower than those from creep tests ($105 \sim 165\ KJ/mol$). Christensen & Das (1973) explained this discrepancy in activation energy values with two reasonings. Firstly, inaccuracies in temperature control and crude measurements during the tests cannot be excluded. Secondly, data from erosion tests cannot be obtained until failure conditions are imminent, thus the activation energy computed from the erosion tests pertains to near-failure conditions. Moreover, Mitchell et al. (1968) have observed that estimated activation energy decreases as failure conditions approach. The calibrated values of number of bonds per unit area based on the BEP datasets ($6.76 \sim 12.65 \times 10^{13}\ m^{-2}$) are comparable to the estimates from creep tests of saturated soils ($\sim 10^{14}$) by Mitchell et al. (1969) and about three orders of magnitudes larger than those from surface and hole erosion tests ($\sim 10^{9}$). This can be attributed to the concentrated seepage pressure under which the local effective stresses in the erosion zones were comparable with those in soils in the creep tests and much larger than the local effective stresses in the soil during surface and hole erosion tests.

CONCLUSIONS

Based on fundamental granular physics, a constitutive model is proposed based on the theory of rate processes to describe BEP progression in GFPI systems. The theory of rate processes has been successfully used in studies of creep, surface and hole erosion of soils, but its applicability to backward erosion piping has not been explored previously. In the derivation of the constitutive model, the concept of flow energy density was adopted, as an alternative to more commonly used hydraulic gradient or hydraulic shear stress measures, due to its capability of better capturing both the initiation and progression phases during BEP, as previously demonstrated in the literature.

The proposed constitutive model was first exercised to perform regression analysis on available experimental data. The values of activation energy and number of bonds per unit area estimated from the experimental data align with the range of values reported in the literature for different processes in soils, and this consistency supports previous finding on applicability of rate of process theory to internal erosion mechanisms. In particular, both BEP and suffusion test data shows that the activation energy estimated through the proposed model provides consistent values for the two different internal erosion mechanisms. This is an interesting finding, because it might lead to a more fundamental understanding of internal erosion phenomena, based on the microgranular effects described through the rate process theory.

To formally evaluate its effectiveness, the rate process-based theoretical model proposed herein was incorporated into a multiphase 1-D numerical framework to simulate progression of BEP. Three independent tests, with different seepage conditions and specimen sizes, were simulated. Three-dimensional seepage flow conditions were shown to influence the simulation of backward erosion piping (Vandenboer et al., 2018). However, as demonstrated by the simulations of experiments performed on 3-D setups (Vandenboer et al. (2019) and Pol et al. (2022)), the observed pipe progression rates were well captured by the proposed framework. Moreover, the values of activation energy and number of bonds per area calibrated with data from independent works are in good agreement with each other, and align with the values estimated from the regression analysis. The numerical results are in good agreement with the experimental observations in both the evolution of local gradients and BEP progression rates. The reported results indicate that the proposed constitutive model brings the potential to be embedded in high-fidelity 3-D numerical frameworks, which is the focus of ongoing research work. The proposed model could also be employed in numerical investigations to provide assessment of backward erosion piping risk and prediction of survivability of flood protection systems under dynamic hydraulic loading conditions.

NOTATION

k_b	Boltzmann's constant
T	absolute temperature
h_p	Planck's constant
R	universal gas constant
ΔF	activation energy
v	frequency of activation
f	force
N	Avogadro constant
λ	distance between successive equilibrium positions
P_{flow}	flow power
$\bar{P}_{flow}$	flow power density
E_{flow}	flow energy
$\bar{E}_{flow}$	flow energy density
V	control volume
S_i	inlet boundary surface
S_o	outlet boundary surface
p	static hydraulic pressure
z	elevation
$\mathbf{v}$	flow velocity
$\mathbf{n}_i$	outer unit normal vector of inlet boundary
$\mathbf{n}_o$	outer unit normal vector of outlet boundary
γ_w	unit weight of water
$\bar{n}$	average number of flow units per unit volume
V_f	average volume of flow unit
m_{fu}	average mass of flow unit
ρ_{dry}	dry bulk density
ρ_s	density of soil particle
S	number of bonds per unit area
α	erosion model parameter 1
β	erosion model parameter 2
h	hydraulic head
k	hydraulic conductivity
D	diffusivity
S_s	specific storage
q	outward flux
h_b	boundary hydraulic head
q_b	boundary flux
γ	concentration of fluidized particles
ϕ	porosity
ϕ_{lim}	limit porosity

REFERENCES

Albalasmeh, A.A. & Ghezzehei, T.A. (2014). Interplay between soil drying and root exudation in rhizosheath development. *Plant and Soil* **374,** 739-751, https://doi.org/10.1007/s11104-013-1910-y.

Andersland, O. & Douglas, A. (1970). Soil deformation rates and activation energies. *Géotechnique* **20,** No. 1, 1-16, https://doi.org/10.1680/geot.1970.20.1.1.

ASTM Standard D4254-16 (2016). Standard test methods for minimum index density and unit weight of soils and calculation of relative density. ASTM International, West Conshohocken, PA, 2016, DOI: 10.1520/D4254-16.

Bagnold, R.A. (1980). An empirical correlation of bedload transport rates in flumes and natural rivers. *Proceedings of the Royal Society of London. A. Mathematical and Physical Sciences* **372,** No. 1751, 453-473, https://doi.org/10.1098/rspa.1980.0122.

Bligh, W.G. (1910). Dams, barrages and weirs on porous foundations. *Engineering News* **64,** No. 26, 708-710.

Brandon, T.L., Batool, A., Jimenez, M., Vroman, N.D. & Corcoran, M.K. (2018). Comparison of levee underseepage analysis methods using blanket theory and finite element analysis. US Army Corps of Engineers, https://doi.org/10.21079/11681/28472.

Christensen, R.W. & Das, B.M. (1973). Hydraulic erosion of remolded cohesive soils. *Highway Research Board Special Report* No. 135.

El Shamy, U. & Aydin, F. (2008). Multiscale modeling of flood-induced piping in river levees. *Journal of Geotechnical and Geoenvironmental Engineering* **134,** No. 9, 1385-1398, https://doi.org/10.1061/(asce)1090-0241(2008)134:9(1385).

Eyring, H. (1936). Viscosity, plasticity, and diffusion as examples of absolute reaction rates. *The Journal of chemical physics* **4,** No. 4, 283-291, https://doi.org/10.1063/1.1749836.

Fascetti, A. & Oskay, C. (2019a). Dual random lattice modeling of backward erosion piping. *Computers and Geotechnics* **105,** 265-276, https://doi.org/10.1016/j.compgeo.2018.08.018.

Fascetti, A. & Oskay, C. (2019b). Multiscale modeling of backward erosion piping in flood protection system infrastructure. *Computer-Aided Civil and Infrastructure Engineering* **34,** No. 12, 1071-1086, https://doi.org/10.1111/mice.12489.

Fleshman, M.S. & Rice, J.D. (2013). Constant gradient piping test apparatus for evaluation of critical hydraulic conditions for the initiation of piping. *Geotechnical Testing Journal* **36,** No. 6, 834-846, https://doi.org/10.1520/gtj20130066.

Fleshman, M.S. & Rice, J.D. (2014). Laboratory modeling of the mechanisms of piping erosion initiation. *Journal of geotechnical and geoenvironmental engineering* **140,** No. 6, 04014017, https://doi.org/10.1061/(asce)gt.1943-5606.0001106.

Foster, M., Fell, R. & Spannagle, M. (2000). The statistics of embankment dam failures and accidents. *Canadian Geotechnical Journal* **37,** No. 5, 1000-1024, https://doi.org/10.1139/t00-030.

Gelet, R. & Marot, D. (2022). Internal erosion by suffusion on cohesionless gap-graded soils: Model and sensibility analysis. *Geomechanics for Energy and the Environment* **31,** 100313, https://doi.org/10.1016/j.gete.2022.100313.

Glasstone, S., Laidler, K.J. & Eyring, H. (1941). *The theory of rate process: The kinetics of chemical reactions, viscosity, diffusion and electrochemical phenomena.* New York and London: McGraw-Hill Book Company, Inc.

Govers, G. (1992). Evaluation of transporting capacity formulae for overland flow. In *Overland flow.* (Parsons, A.J. & Abrahamls, A.D. (eds.)) pp. 224-261. London, UK: CRC Press, https://doi.org/10.1201/b12648-17.

Gularte, R.C., Kelly, W. & Nacci, V. (1980). Erosion of cohesive sediments as a rate process. *Ocean Engineering* **7,** No. 4, 539-551, https://doi.org/10.1016/0029-8018(80)90051-7.

International Commission on Large Dams (2013). ICOLD Bulletin 164 on internal erosion of dams, dikes and levees and their foundations.

Kodieh, A., Gelet, R., Marot, D. & Fino, A. (2021). A study of suffusion kinetics inspired from experimental data: comparison of three different approaches. *Acta Geotechnica* **16,** No., 347-365, https://doi.org/10.1007/s11440-020-01016-5.

Kuang, X., Jiao, J.J., Zheng, C., Cherry, J.A. & Li, H. (2020). A

review of specific storage in aquifers. *Journal of Hydrology* **581,** p.124383, https://doi.org/10.1016/j.jhydrol.2019.124383.

Marchi, M., Martínez, M.F.G., Gottardi, G. & Tonni, L. (2021). Field measurements on a large natural sand boil along the river Po, Italy. *Quarterly Journal of Engineering Geology and Hydrogeology* **54,** No. 4, qjegh2020-097, https://doi.org/10.1144/qjegh2020-097.

Marot, D., Le, V.D., Garnier, J., Thorel, L. & Audrain, P. (2012). Study of scale effect in an internal erosion mechanism: centrifuge model and energy analysis. *European Journal of Environmental and Civil Engineering* **16,** No. 1, 1-19, https://doi.org/10.1080/19648189.2012.667203.

Matsui, T., Abe, N., Mitchell, J.K. & Ito, T. (1980). Microscopic study of shear mechanisms in soils. *Journal of the Geotechnical Engineering Division* **106,** No. 2, 137-152, https://doi.org/10.3208/sandf1972.14.29.

Michalowski, R., Wang, Z. & Nadukuru, S. (2018). Maturing of contacts and ageing of silica sand. *Géotechnique* **68,** No. 2, 133-145, https://doi.org/10.1680/jgeot.16.p.321.

Mitchell, J.K. (1964). Shearing resistance of soils as a rate process. *Journal of the Soil Mechanics and foundations Division* **90,** No. 1, 29-61, https://doi.org/10.1016/0022-4898(64)90023-0.

Mitchell, J.K., Campanella, R.G. & Singh, A. (1968). Soil creep as a rate process. *Journal of the Soil Mechanics and Foundations Division* **94,** No. 1, 231-253, https://doi.org/10.1061/jsfeaq.0001085.

Mitchell, J.K., Singh, A. & Campanella, R.G. (1969). Bonding, effective stresses, and strength of soils. *Journal of the Soil Mechanics and Foundations Division* **95,** No. 5, 1219-1246, https://doi.org/10.1016/0022-4898(70)90065-0.

Mitchell, J.K. & Soga, K. (2005). *Fundamentals of soil behavior.* Hoboken, NJ, USA: John Wiley & Sons.

Murayama, S., Michihiro, K. & Sakagami, T. (1984). Creep characteristics of sands. *Soils and foundations* **24,** No. 2, 1-15, https://doi.org/10.3208/sandf1972.24.2_1.

Murayama, S. & Shibata, T. (1961). Rheological properties of clays. *Proc. 5th ICSMFE.* 269-273.

Negrinelli, G. (2015). *Investigation of the process of seepage and backward erosion piping under dikes in heterogeneous sands.* PhD Thesis, University of Brescia, Brescia, Italy.

Negrinelli, G., van Beek, V., & Ranzi, R. (2016). Experimental and numerical investigation of backward erosion piping in heterogeneous sands. *Scour and Erosion: Proceedings of the 8th International Conference on Scour and Erosion*. CRC Press, Oxford, 473–482.

Ojha, C., Singh, V. & Adrian, D. (2003). Determination of critical head in soil piping. *Journal of Hydraulic Engineering* **129,** No. 7, 511-518, https://doi.org/10.1061/(asce)0733-9429(2003)129:7(511).

Ovalle-Villamil, W. & Sasanakul, I. (2021). Centrifuge modeling study of backward erosion piping with variable exit size. *Journal of Geotechnical and Geoenvironmental Engineering* **147,** No. 11, 04021114, https://doi.org/10.1061/(asce)gt.1943-5606.0002642.

Papamichos, E. & Vardoulakis, I. (2005). Sand erosion with a porosity diffusion law. *Computers and Geotechnics* **32,** No. 1, 47-58, https://doi.org/10.1016/j.compgeo.2004.11.005.

Peng, S. & Rice, J.D. (2020). Measuring critical gradients for soil loosening and initiation of backward erosion-piping mechanism. *Journal of Geotechnical and Geoenvironmental Engineering* **146,** No. 8, 04020069, https://doi.org/10.1061/(ASCE)GT.1943-5606.0002277.

Pol, J.C., Kanning, W., van Beek, V.M., Robbins, B.A., & Jonkman, S.N. (2022). Temporal evolution of backward erosion piping in small-scale experiments. *Acta Geotechnica* **17,** No. 10, 4555-4576, https://doi.org/10.1007/s11440-022-01545-1.

Powell, T. & Richerson, P.J. (1985). Temporal Variation, Spatial Heterogeneity, and Competition for Resources in Plankton Systems: A Theoretical Model. *The American Naturalist* **125,** No. 3, 431-464, https://doi.org/10.1086/284352.

Raudkivi, A. & Hutchison, D. (1974). Erosion of kaolinite clay by flowing water. *Proceedings of the Royal Society of London. A. Mathematical and Physical Sciences* **337,** No. 1611, 537-554, https://doi.org/10.1098/rspa.1974.0066.

Reddi, L.N., Bonala, M. & Lee, I. (2000). Comparison of internal and surface erosion using flow pump tests on a sand-kaolinite mixture. *Geotechnical testing journal* **23,** No. 1, 116-122, https://doi.org/10.1520/gtj11129j.

Richards, K.S. & Reddy, K.R. (2012). Experimental investigation of initiation of backward erosion piping in soils. *Géotechnique* **62,** No. 10, 933-942, https://doi.org/10.1680/geot.11.p.058.

Richards, K.S. & Reddy, K.R. (2007). Critical appraisal of piping phenomena in earth dams. *Bulletin of Engineering Geology and the Environment* **66,** 381-402, https://doi.org/10.1007/s10064-007-0095-0.

Riha, J., & Petrula, L. (2023). Experimental Research on Backward Erosion Piping Progression. *Water* **15,** No. 15, 2749, https://www.mdpi.com/2073-4441/15/15/2749.

Robbins, B. & Griffiths, D. (2021). A two-dimensional, adaptive finite element approach for simulation of backward erosion piping. *Computers and Geotechnics* **129,** 103820, https://doi.org/10.1016/j.compgeo.2020.103820.

Robbins, B.A. (2016). Numerical modeling of backward erosion piping. *Applied numerical modeling in geomechanics* **2016,** 551-558.

Robbins, B.A., Stephens, I.J., Van Beek, V.M., Koelewijn, A.R. & Bezuijen, A. (2020). Field measurements of sand boil hydraulics. *Géotechnique* **70,** No. 2, 153-160, https://doi.org/10.1680/jgeot.18.p.151.

Robbins, B.A., van Beek, V.M., López-Soto, J.F., Montalvo-Bartolomei, A.M. & Murphy, J. (2018). A novel laboratory test for backward erosion piping. *International Journal of Physical Modelling in Geotechnics* **18,** No. 5, 266-279, https://doi.org/10.1680/jphmg.17.00016.

Sail, Y., Marot, D., Sibille, L., $ Alexis, A. (2018). Suffusion tests on cohesionless granular matter: experimental study. *European Journal of Environmental and Civil Engineering* **15,** No. 5, 799-817, https://doi.org/10.1080/19648189.2011.9693366.

Saltelli, A., Ratto, M., Andres, T., Campolongo, F., Cariboni, J., Gatelli, D., Saisana, M. & Tarantola S. (2008). *Global sensitivity analysis: the primer.* West Sussex, UK: John Wiley & Sons.

Schmertmann, J.H. (2000). The no-filter factor of safety against piping through sands. In *Judgment and innovation: the heritage and future of the geotechnical engineering profession.* (Silva, F. & Kavazanjian Jr., E. (eds.)) pp. 65-132. Reston, VA: ASCE, https://doi.org/10.1061/9780784405376.006.

Sellmeijer, H., de la Cruz, J.L., van Beek, V.M. & Knoeff, H. (2011). Fine-tuning of the backward erosion piping model through small-scale, medium-scale and IJkdijk experiments. *European Journal of Environmental and Civil Engineering* **15,** No. 8, 1139-1154, https://doi.org/10.1080/19648189.2011.9714845.

Sellmeyer, J.B. (1988). *On the mechanism of piping under impervious*

structures. PhD Thesis, Delft University of Technology, Delft, Netherlands.

Sibille, L., Lominé, F., Poullain, P., Sail, Y. & Marot, D. (2015). Internal erosion in granular media: direct numerical simulations and energy interpretation. *Hydrological Processes* **29,** No. 9, 2149-2163, https://doi.org/10.1002/hyp.10351.

Sterpi, D. (2003). Effects of the erosion and transport of fine particles due to seepage flow. *International journal of Geomechanics* **3,** No. 1, 111-122, https://doi.org/10.1061/(asce)1532-3641(2003)3:1(111).

Teunissen, P.J.G. (1990). Nonlinear least squares. *Manuscripta Geodaetica* **15,** 137-150.

Thomas, J.W. (2013). *Numerical partial differential equations: finite difference methods.*New York, USA: Springer.

van Beek, V., Van Essen, H., Vandenboer, K. & Bezuijen, A. (2015). Developments in modelling of backward erosion piping. *Géotechnique* **65,** No. 9, 740-754, https://doi.org/10.1680/geot.14.p.119.

van Beek, V.M. (2015). *Backward erosion piping: Initiation and progression.* PhD Thesis, Delft University of Technology, Delft, Netherlands.

van Beek, V.M., De Bruijn, H., Knoeff, J., Bezuijen, A. & Förster, U. (2010). Levee failure due to piping: A full-scale experiment. In: *Proceedings 5th International Conference on Scour and Erosion (ICSE-5).* (Burns, S.E., Bhatia, S.K., Avila, C.M.C. & Hunt, B.E. (eds.)). San Francisco, USA: ASCE, https://doi.org/10.1061/41147(392)27.

van Beek, V.M., Knoeff, H. & Sellmeijer, H. (2011). Observations on the process of backward erosion piping in small-, medium-and full-scale experiments. *European Journal of Environmental and Civil Engineering* **15,** No. 8, 1115-1137, https://doi.org/10.1080/19648189.2011.9714844.

Vandenboer, K., van Beek, V. & Bezuijen, A. (2014). 3D finite element method (FEM) simulation of groundwater flow during backward erosion piping. *Frontiers of Structural and Civil Engineering* **8,** 160-166, https://doi.org/10.1007/s11709-014-0257-7.

Vandenboer, K., Van Beek, V. & Bezuijen, A. (2018). 3D character of backward erosion piping. *Géotechnique* **68,** No. 1, 86-90, https://doi.org/10.1680/jgeot.16.p.091.

Vandenboer, K., Celette, F., & Bezuijen, A. (2019). The effect of sudden critical and supercritical hydraulic loads on backward erosion piping: small-scale experiments. *Acta Geotechnica* **14,** 783-794, https://doi.org/10.1007/s11440-018-0756-0.

Wang, Y. & Ni, X. (2013). Hydro-mechanical analysis of piping erosion based on similarity criterion at micro-level by PFC3D. *European Journal of Environmental and Civil Engineering* **17,** No. sup1, s187-s204, https://doi.org/10.1080/19648189.2013.834594.

Wang, Z. (2017). *Contact maturing and aging of silica sand.* PhD Thesis, University of Michigan, Ann Arbor, MI.

White, F.M. (1999). Open Channel Flow. In *Fluid Mechanics.*(Kreith, F (ed.)) pp. 65-73. Boca Raton, FL: CRC Press.

Zhang, X., Wong, H., Leo, C.J., Bui, T.A., Wang, J., Sun, W. & Huang,Z. (2013). A thermodynamics-based model on the internal erosion of earth structures. *Geotechnical and Geological Engineering* **31,** No., 479-492, https://doi.org/10.1007/s10706-012-9600-8.